Dynamics of Rare Gases in Zeolites: Instantaneous Normal Mode Analysis

Vishal Mehra,[†] Ritu Basra, Monika Khanna, and Charusita Chakravarty*

Department of Chemistry, Indian Institute of Technology—Delhi, Hauz Khas, New Delhi 110016, India

Received: August 27, 1998; In Final Form: January 28, 1999

The instantaneous normal mode (INM) spectra of rare gases in zeolites is analyzed with a view to understanding the short-time dynamical behavior of fluids adsorbed in confining media. Xenon adsorption in all-silica polymorphs of four zeolites (silicalite, mordenite, zeolite-A, and zeolite-Y) is studied using molecular dynamics and Monte Carlo simulations. The participation ratio distribution is shown to be a particularly good indicator of the extent of ballistic behavior in the short-time dynamics. The fraction of imaginary modes in the INM spectrum is shown to be correlated with the self-diffusion coefficient; however, a significant number of imaginary modes would appear to be due to the negative curvature of the confining potential rather than to the existence of barrier crossing motions. The Einstein frequency shows interesting temperature-dependent behavior which is sensitive to the structure and framework density of the zeolite. The gradual emergence of liquidlike behavior with increasing concentration is reflected in both the participation ratio distribution and the harmonicity ratio; these features of the INM spectrum are therefore expected to be useful for indexing the modification of dynamical behavior of a fluid on confinement.

1. Introduction

Dynamics of sorbate molecules in microporous and mesoporous media is of interest from the point of view of catalysis and separation. Porous media can range from highly ordered crystalline structures such as zeolites to random media such as carbon blacks and Vycor. While the chemistry and physics of complex and/or reactive sorbates such as saturated and unsaturated long-chain hydrocarbons are of greatest interest industrially, even the study of rare gas adsorption in zeolites and other microporous media reveals a surprisingly diverse range of effects due to confinement on structural and dynamical properties.[1,2] Computer simulations have played an important role in developing an understanding of the microscopic behavior of such complex sorbate−sorbent systems.[3−6] In particular, the dynamics of rare gases, Ne, Ar, Kr, and Xe, in various zeolites have been extensively studied by both computational tools such as microcanonical molecular dynamics, as well as experimental, for example, using Xe^{129} NMR studies.[7−11] Despite the relative simplicity of these systems, interesting dynamical phenomena have been uncovered such as the levitation effect in which sorbates of a specific size range diffuse unusually rapidly through zeolites.

In this paper we correlate dynamics of rare gases in zeolites with an equilibrium property of the system—the instantaneous normal mode spectrum. The instantaneous normal mode (INM) spectrum is obtained as the set of normal mode frequencies associated with configurations sampled from some suitable ensemble. Since at finite temperatures the configurations will not correspond exactly to local minima on the potential energy surface (PES), the INM spectrum will have real and imaginary branches indicating the extent to which positive and negative curvature regions respectively are sampled by the system. The INM frequencies will be related to the short-time dynamics since, for sufficiently small displacements and therefore for sufficiently small times, a quadratic expansion of the potential about any reference configuration will be adequate. This has motivated the development of INM analysis as a tool to understand liquid-state dynamics and solvation.[12,13] Translational and rotational velocity autocorrelation functions for molecular liquids can be reproduced for time scales of less than a picosecond from INM data.[14] The degree of delocalization of the imaginary branch modes can be correlated with the onset of glassy behavior.[15] Based on Zwanzig's model of self-diffusion in which a liquid hops between local minima on the PES with a lifetime in each minima described by some survival time distribution, Keyes and co-workers have derived long-time dynamical properties, such as the diffusion coefficient, from the INM spectrum.[16−19] The Lyapunov spectra of Lennard−Jones liquids can also be derived from the INM spectrum with the aid of a reasonable estimate of the decorrelation time.[20] However, connecting the INM data to such long-time averaged dynamical quantities as the diffusion constants or Lyapunov spectra requires additional assumptions about the nature of liquid-state dynamics and is therefore more controversial.[21] Despite this caveat, simulations on a wide range of systems, including atomic clusters, molecular liquids, liquid metals, and ionic melts, have indicated that the INM spectrum is a useful indicator of dynamical behavior.[22−27] This is particularly convenient for systems or phenomena for which a reliable dynamical simulation method does not exist. For example, for quantum many-body systems, path integral methods provide a way to simulate static but not dynamic properties. Since the INM spectrum is an equilibrium quantity it can be computed for a quantum system and is relevant since there is no reliable simulation method for many-body quantum dynamics.[28,29] In the case of classical systems, for many problems such as adsorption or phase transitions, ensembles other than the microcanonical are convenient.[30,31] While molecular dynamics schemes can be set up in other ensembles, such as the canonical or the isothermal−isobaric, the interpretation of the simulation

* Author to whom correspondence should be addressed.

[†] Present Address: Departamento de Fisica, Universidad Federal de Sao Carlos, Via Washington Luiz km 235, 13565-905, Caixa Postal 676, Sao Carlos, SP, Brazil.

10.1021/jp983544k CCC: $18.00
Published on Web 03/23/1999

dynamics in terms of the physical motion of the molecules can become tricky because of the fictitious dynamics associated with macroscopic variables such as the temperature and pressure. The INM spectrum, however, can be computed in any ensemble and may therefore be useful in such situations.

The quenched normal modes (QNM) associated with a given instantaneous configuration are obtained by using a steepest-descent type technique to locate the nearest local minimum and then computing the normal modes associated with this inherent structure. It is useful to compare INM and QNM spectra; the two coincide at 0 K, and the differences at higher temperatures indicate the ability of the system to explore different regions of the PES as a consequence of the thermal kinetic energy. Quenched normal mode spectra and inherent structure analysis have a long history in the simulation of liquids and glasses.[32] The quenched energies and normal modes provide an idea of the local minima on the PES sampled by the system. The observation by Stillinger that in simulations of liquids the system jumped between different local minima led Zwanzig to formulate the self-diffusion model mentioned above.

Confinement of a liquid in a porous medium will modify the dynamical behavior, the extent of modification depending on factors such as the pore volume, strength of interaction between adsorbed fluid and adsorbent, concentration of adsorbate, and geometrical features of the adsorbing host. If concentrations are low and sorbate−sorbent interactions are large, short-time dynamics of the sorbate will be ballistic rather than diffusional. By varying the porous medium and the adsorbate concentration one should be able to generate a range of behavior in the short-time dynamics from purely ballistic to purely diffusional. To test the usefuless of INM spectra for obtaining dynamical information for this class of systems, we decided to study rare gas dynamics in zeolites using both Monte Carlo and molecular dynamics. Since the latter technique provides accurate dynamical information in the microcanonical ensemble, comparisons between the "exact" behavior and various INM quantities can be made. Moreover, it is known that rare gases adsorbed in zeolites undergo ballistic motion on short time scales and a crossover to diffusional motion takes place typically at about 1ps. Short-time dynamics in zeolites at low concentrations will therefore exhibit almost pure ballistic character in contrast to the diffusional behavior in simple liquids. A couple of studies have previously computed INM spectra for sorbates in zeolites.[33−35] To our knowledge, however, this is the first work to implement a systematic INM/QNM analysis of rare gas dynamics in zeolites with a view to determining signatures due to confinement.

We examine xenon adsorption in all-silica polymorphs of four zeolites: silicalite (ZSM-5), faujasite (zeolite-Y), mordenite, and Na-A (zeolite-A). All four have been studied before by molecular dynamics and/or Monte Carlo methods; therefore, physically reasonable potential energy surfaces are available. By using the purely siliceous compositional variants, we can test the effect of differing pore volume and channel geometries while avoiding the additional complexities associated with disordered siting of cations in aluminum-containing zeolites and strong induction energy contributions to the zeolite−sorbate interaction. We also assume that the zeolite lattice is rigid and merely provides a confining potential; this has been shown to be a reasonable approximation for rare gas sorption. In section 2, we describe the zeolite structures and potential energy surfaces used in this study. The features of the instantaneous and quenched mode spectra relevant for this work are summarized in section 3. Computational details are described in section 4. Results are presented and discussed in section 5. Section 6 contains conclusions.

2. Zeolite Structures and Potential Energy Surfaces

The potential energy surface for the rare gas−zeolite interaction was based on the Kiselov model.[36−38] The Kiselov model assumes that the Si/Al atoms of the lattice are effectively shielded from interaction with the sorbate by the oxygen tetrahedra. Zero charge is ascribed to the Si and Al atoms. The positive charges on the framework cations are compensated by assigning partial charges to the framework oxygen atoms. The interaction between the zeolite framework and a simple sorbate such as a rare gas atom is then assumed to consist of two components: a dispersion term and an electrostatic induction term. The Kiselov model has been extensively used in simulations of sorbate−zeolite systems and, despite its simplicity, found to provide reasonable results in comparison with experiment.[3−42]

For purely siliceous forms of the zeolites, there are no framework cations and therefore preservation of electroneutrality does not require assigning of partial charges on lattice oxygens. This removes the contribution of the induction term to the potential energy. The dispersion contribution is written as

$$V_{\mathrm{D}} = 4\epsilon_{\mathrm{OR}}\sum_{j}\left(\frac{\sigma_{\mathrm{OR}}^{12}}{r_{ij}^{12}} - \frac{\sigma_{\mathrm{OR}}^{6}}{r_{ij}^{6}}\right) \tag{1}$$

where j represents summation over all framework atoms, r_{ij} is the distance between a sorbate atom i and a framework atom j, and ϵ_{OR} and σ_{OR} are the Lennard−Jones well depth and size parameters, respectively, for the rare gas−oxygen dispersion interaction. The van der Waals minimum, r_{OR}, for the oxygen−rare gas bond is assumed to be the sum of the van der Waals radii for the two atoms; then $\sigma_{\mathrm{OR}} = 2^{-1/6}r_{\mathrm{OR}}$. The well depth, ϵ_{OR}, of the Lennard−Jones potential is given in CGS units by

$$\epsilon_{\mathrm{OR}} = \frac{3e^2a^{1/2}{}_0\alpha_{\mathrm{O}}\alpha_{\mathrm{R}}}{8\sigma_{\mathrm{OR}}^6(\sqrt{\alpha_{\mathrm{O}}/n_{\mathrm{O}}} + \sqrt{\alpha_{\mathrm{R}}/n_{\mathrm{R}}})} \tag{2}$$

where α_i is th static polarizability of atom i, i = O or R, and n_i is the number of electrons of atom i. The total potential enery of the system is subdivided into a guest−host term, U_{gh}, obtained by summing over dispersion interactions with the lattice of all sorbate atoms, and a guest−guest term, U_{gg}, which is a pairwise Lennard−Jones interaction between the sorbate atoms.

Diffusion of xenon in all-silica polymorphs of ZSM-5, mordenite, zeolite-Y, and zeolite-A were studied. Structural data for each zeolite relevant for MD and MC simulations are given in Table 1. Silicalite, $Si_{96}O_{192}$, is the pure silica form of the industrially important high-silica zeolite ZSM-5. The structure has been taken from the crystallographic data for the orthorhombic form.[43] The naturally occurring form of zeolite-Y is the aluminosilicate sodalite.[44] The pure-silica form of this zeolite can be prepared from nonaqueous solvent sysems.[45] Following ref 46, we construct the silica-sodalite structure by replacing all aluminum atoms by silicon atoms in the Na-Y structure and removing the sodium atoms from the unit cell.[47] An all-silica analogue of Zeolite-A was constructed similarly from crystallographic data for Na-A.[48] Dehydrated mordenite, $Na_8Al_8Si_{40}O_{96}$, is stable to acid leaching and therefore can be de-aluminated almost completely. Unit cell parameters and structure of siliceous mordenite were taken from ref 49.

TABLE 1: Structural Data for Zeolites[a]

zeolite	unit cell composition	lattice parameters			space group	simulation cell	framework density[b]
		a (Å)	*b* (Å)	*c* (Å)			
silicalite	$Si_{96}O_{192}$	20.07	19.92	13.42	Pnma	(1,1,2)	17.9
mordenite	$Si_{48}O_{96}$	18.13	20.49	7.52	CmCm	(1,1,3)	17.2
zeolite-A	$Si_{192}O_{384}$	24.55	24.55	24.55	$Fm\bar{3}c$	(1,1,1)	12.9
zeolite-Y	$Si_{192}O_{384}$	24.85	24.85	24.85	$Fd\bar{3}m$	(1,1,1)	12.7

[a] Compositions are for the all-silica polymorphs. [b] Framework densities given in units of number of tetrahedral (T) atoms per 1000 Å.^{3}

We have effectively taken two low-density and two high-density zeolites. Zeolites A and Y are expected to show very similar behavior since the α-cage subunit is common to both. We used a common set of PES parameters for all the siliceous zeolites since the purpose was to compare the effect of different confining structures on the instantaneous and quenched normal mode spectra rather than to accurately fit specific experimental quantities such as Henry's constants and heats of adsorption. The Lennard−Jones parameters for the Xe−Xe interaction were taken from the literature as 221 K and 4.1 Å.[50] The Xe−O parameters for all four zeolites were taken from those parametrized for silicalite as $\epsilon = 209$ K and 3.28 Å.[38] This parametrization was done based on eq 2 and the oxygen atom polarizabilities and radius in silicalite were chosen to reproduce the temperature dependence of the Henry constants. PE contour plots with these parameters were compared to those given for Zeolite-Y and mordenite in ref 46. The size of the simulation cells was chosen in order to converge the guest−host potential energy to within 2% at 100 K. Since the zeolite cage was treated as a rigid, confining lattice, no potential parameters for the Si−O bonds were required.

3. Instantaneous and Quenched Normal Mode Analysis

An instantaneous normal-mode analysis is performed by expanding the potential energy function to second order in the displacement, $\mathbf{r}(t) - \mathbf{r}(0)$, where $\mathbf{r}(0)$ is the initial configuration of the N-particle system at time $t = 0$ and $\mathbf{r}(t)$ is the configuration after a short interval of time t. The short-time classical Hamiltonian can then be written as

$$H \approx \sum_{i=1}^{3N} \frac{m_i}{2}\left(\frac{\mathrm{d}r_i}{\mathrm{d}t}\right)^2 + V(\mathbf{r}(0)) - \mathbf{F}'(\mathbf{r}(t) - \mathbf{r}(0)) + 0.5(\mathbf{r}(t) - \mathbf{r}(0))^T \mathbf{D}'(\mathbf{r}(t) - \mathbf{r}(0)) \quad (3)$$

where $\mathbf{F}'$ is the vector representing the forces acting on the system at $t = 0$ and $\mathbf{D}'$ is the second-derivative matrix or Hessian of the potential evaluated at $\mathbf{r}(0)$. Converting to mass-weighted coordinates, $z_i = \sqrt{m_i} r_i$,

$$H \approx \sum_{i=1}^{3N} \frac{1}{2}\left(\frac{\mathrm{d}z_i}{\mathrm{d}t}\right)^2 + V(\mathbf{r}(0)) - \mathbf{F}(\mathbf{z}(t) - \mathbf{z}(0)) + 0.5(\mathbf{z}(t) - z(0))^T \mathbf{D}(\mathbf{z}(t) - z(0)) \quad (4)$$

where the derivative matrixes $\mathbf{F}$ and $\mathbf{D}$ are constructed with respect to the mass-weighted coordinates. The Hessian matrix can be diagonalized to give the eigenvalues, $\{\omega_i^2, i = 1, 3N\}$, and eigenvectors $\mathbf{U}(\mathbf{r}(0))$. The eigenvalues correspond to the squares of the normal-mode frequencies. As mentioned in the Introduction since an instantaneous configuration need not necessarily (in fact at finite temperature is almost never) exactly at a minimum in the PES, therefore there will always be a set of imaginary frequency normal modes. Conventionally the imaginary branch is depicted on the negative frequency axis.

The INM spectrum or the normalized INM density of states is obtained by averaging the INM frequencies over a set of configurations sampled from the equilibrium distribution in any ensemble. Mathematically, it may be represented as

$$\rho(\omega) = \langle (1/3N) \sum_{i=1}^{3N} \delta(\omega - \omega_i) \rangle \quad (5)$$

If the system has any collective translational or rotational modes, as in the case of a cluster or a liquid, they are removed from this distribution. For rare gas atoms moving within a rigid zeolite framework, such zero-frequency modes are absent and therefore no modes need to be explicitly removed from the INM distribution. Several features of the INM spectrum can be correlated with the dynamical behavior of the system, particularly in the short-time limit. For example, the fraction of imaginary modes, F_{imag}, indicates the extent to which the system samples regions of negative curvature, including barrier and shoulder regions of the PES. The Einstein frequency, ω_{E}, is defined as: $\omega_{\mathrm{E}}^2 = \int \omega^2 \rho(\omega)\, \mathrm{d}\omega$ where $\rho(\omega)$ is the normalized INM spectrum. Since $\omega_{\mathrm{E}}^2 = \langle V'' \rangle / m3N$ where $\langle V'' \rangle$ is the ensemble average of the trace of the Hessian $\mathbf{D}'$ the Einstein frequency is a measure of the average force constant, $\langle V'' \rangle$, of the system. ω_{E} can be decomposed into real, ω_{R}, and imaginary, ω_{I}, components such that

$$\omega_{\mathrm{E}}^2 = (1 - F_{\mathrm{imag}})\omega_{\mathrm{R}}^2 + F_{\mathrm{imag}}\omega_{\mathrm{I}}^2 \quad (6)$$

where F_{imag} is the fraction of imaginary frequencies. An interesting quantity associated with INM analysis is the participation ratio which measures the number of atoms participating in that normal mode. An eigenvector representing the αth instantaneous normal mode associated with some configuration is denoted by $\mathbf{q}_\alpha = \{U_{\alpha j}, j = 1, 3N\} = \{U_{\alpha ix}, U_{\alpha iy}, u_{\alpha iz}, i = 1, N\}$ where in the second notation the Cartesian coordinates of each atom i are explicitly indicated. The participation ratio is then defined as[51]

$$P_\alpha = \frac{1}{(\sum_{k=1}^{N} (U_{\alpha kx}^2 + U_{\alpha ky}^2 + U_{\alpha kz}^2)^2)} \quad (7)$$

In the normalization convention defined above, for a completely delocalized mode all the components of the eigenvector will equal $\pm 1/\sqrt{3N}$ and $P_\alpha = N$. For a localized mode involving only one atom, $P_\alpha = 1$. This convention is useful if one wishes to identify the number of atoms participating in a given mode and has been used to compare the relative degree of delocalization of INMs in different frequency ranges for a number of liquids and glasses. A participation ratio distribution, $P(\omega)\mathrm{d}\omega$, representing the average participation ratio associated with INMs lying in the frequency range ω to $\omega + \mathrm{d}\omega$ can be calculated by ensemble averaging. It should be noted, however, that to rigorously identify the truly delocalized modes which extend

essentially over the entire simulation cell, it is necessary to do a finite-size scaling study and normalize the participation ratio as $P'_\alpha = P_\alpha/N$. With this normalization, the true delocalized modes will have P'_α of the order of unity regardless of system size, whereas the modes involving localized clusters of atoms will have $P'_\alpha \rightarrow 0$ as $N \rightarrow \infty$.

The properties discussed above are features of the equilibrium INM spectrum and can be defined in any ensemble and for both quantum and classical systems. Unlike in many of the studies of INMs in liquids, in this study we do not attempt to quantitatively reproduce the diffusion constant, which is a long-time averaged property, from the INM spectrum. However, for a classical system, it is possible to further analyze the short-time dynamics in terms of the kinematics of the normal mode coordinates. By using the INM modes, $U(\mathbf{r}(0))$ for some configuration, $\mathbf{r}(0)$, one can rewrite the Hamiltonian as

$$H \approx V(\mathbf{r}(0)) + \sum_{i=1}^{3N}\left(\frac{1}{2}\left(\frac{dq_i}{dt}\right)^2 + \frac{1}{2}\omega_i^2 q_i^2 - f_i q_i\right) \qquad (8)$$

where $f_i(\mathbf{r}(0)) = \sum_j U_{ij}F_i$ and $q_i(t, \mathbf{r}(0)) = \sum_j U_{ij}\{z_j(t) - z_j(0)\}$. To remove the term linear in $\{q_i\}$ from the Hamiltonian, one can define shifted normal mode coordinates, $x_i = q_i - (f_i/\omega_i^2)$, such that

$$H \approx V(\mathbf{r}(0)) + \sum_{i=1}^{3N}\left(\frac{1}{2}\left(\frac{dx_i}{dt}\right)^2 + \frac{1}{2}\omega_i^2 x_i^2 - (f_i^2/2\omega_i^2)\right) \qquad (9)$$

$|f_i/\omega^2{}_i|$ can be interpreted as the displacement of the normal mode coordinate from its nearest extremum: minimum in the case of stable modes with $\omega_i^2 > 0$ and maximum in the case of unstable modes with $\omega_i < 0$. For the stable modes, if the harmonic picture were applicable, the canonical ensemble average of $|f/\omega^2|$ will be proportional to $\sqrt{k_B T}/\omega$ and the slope of $\log|f/\omega^2|$ versus $\log \omega$ should be -1. Alternatively, if f were constant with ω, then the corresponding slope should be -2. We term the ratio $|f/\omega^2|$ as the harmonicity ratio. For water, both the stable and unstable modes show a linear dependence with slopes of -1.44 and -1.9 respectively.[22] The time evolution of the shifted normal modes and the corresponding velocities are given by

$$x_i(t) = x_i(0)\cos(\omega_i t) - (v_i(0)/\omega_i)\sin(\omega_i t)$$

$$v_i(t) = v_i(0)\cos(\omega_i t) - \omega_i x_i(0)\sin(\omega_i t)$$

Using these relations for the time evolution and assuming a Maxwell−Boltzmann distribution of velocities at $t = 0$, Stratt et al. have shown that the velocity autocorrelation function is given by:

$$C_{vv}(t) = \int \rho(\omega)\cos(\omega t)d\omega$$

$$= 1 - \frac{\langle\omega^2\rangle}{2!}t^2 + \frac{\langle\omega^4\rangle}{4!}t^4 + \ldots \qquad (10)$$

where $\langle\omega^n\rangle = \int \omega^n\rho(\omega)d\omega$. For simple nonpolar and dipolar liquids, the short time behavior of the translational autocorrelation function was well reproduced by the above formula provided only stable modes were used for evaluating the integral.

4. Computational Details

The Metropolis algorithm was employed for the canonical ensemble Monte Carlo simulations. Since the zeolite lattice was held rigid, only the xenon atom positions were changed when generating trial moves. Run lengths of 100 000 to 800 000 trial moves were used depending on temperature and concentration. Acceptance ratios were kept between 40% and 50%. Orthorhombic periodic boundary conditions were used for all four zeolites with simulation cell dimensions as given in Table 1. INM spectra were calculated every 20 to 100 trial moves. Quenches were carried out after every 100 MC moves by taking the current configuration in the Metropolis walk and applying a multidimensional minimization procedure to move the system to the nearest local minimum on the PES. To avoid numerical instabilities associated with a finite cutoff for Lennard−Jones type interactions, instead of conjugate gradient minimization techniques, Powell's quadratically convergent direction set algorithm was used which does not require the first-derivatives of the PES.[52]

Molecular dynamics simulations were carried out in the microcanonical ensemble using the velocity Verlet algorithm. Initial velocities were sampled from a Maxwell−Boltzmann distribution corresponding to some preset temperature, and temperature scaling was carried out during the equilibriation period. A time step of 500 a.u. (12 fs) was shown to conserve energy to the fourth significant figure for a run length of 1.44 ns. Time steps of 500 to 1000 a.u. were therefore used in all the MD simulations. Boundary conditions and simulation cell dimensions are the same as in the Monte Carlo simulations. As mentioned before, positions of the zeolite atoms were held fixed and only the sorbate atoms were moved using the MD algorithm. Sorbate mass was taken as 131 amu. Positions and velocities were stored every 10 time steps. Instantaneous normal modes were calculated at intervals of 100 time steps. The INM spectra results from MD at the average temperature of the run, T_r, coincided with canonical MC results at the same temperature within the error bars of the simulation. Diffusion coefficients were calculated using two different methods: (i) according to the Einstein relation

$$D = \langle|r_i(t) - r_i(0)|^2\rangle/6t \qquad (11)$$

and (ii) by integration of the velocity autocorrelation function

$$D = (1/3)\int_0^{t_{max}} dt\langle v_i(t)v_i(0)\rangle \qquad (12)$$

Integration of the above equation was done using trapezoidal quadrature. Convergence of the diffusion coefficient was tested with respect to run length and runs of 1.5 ns were found to be sufficient for temperatures above 400 K. For lower temperatures, longer run lengths were used.

5. Results and Discussion

We first present our results for the velocity autocorrelation functions and diffusion constants which were obtained from molecular dynamics runs. The short-time dynamics of the system is reflected in the behavior of $C_{vv}(t)$ for t less than a picosecond. The diffusion coefficient reflects the long-time averaged dynamical behavior of the system. Figure 1 shows the behavior of $C_{vv}(t)$ in different zeolites for the first 10 ps. Notice that the first minimum in $C_{vv}(t)$ at low temperatures occurs at approximately 1 ps which is much larger than the corresponding value of 0.2 ps for a typical liquid such as Ar. This time scale represents approximately the time taken to rebound from the zeolite wall rather than from the solvent cage. The oscillations in $C_{vv}(t)$ are much more pronounced in the case of silicalite than zeolite-Y because of the narrower channel structure. With

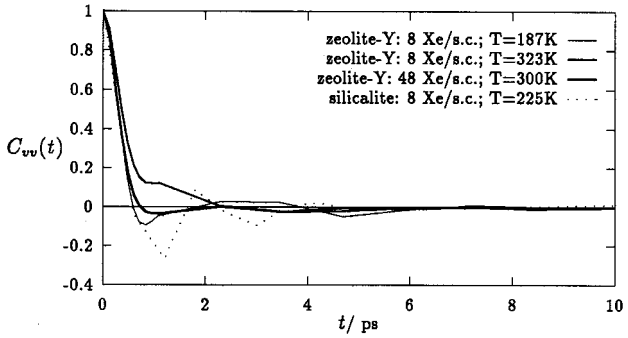

Figure 1. Short-time behavior of velocity autocorrelation function, $C_{vv}(t)$, for xenon in zeolite-Y and silicalite.

TABLE 2: Molecular Dynamics Results for the Diffusion Coefficient, *D*, the Average Potential Energy, $\langle U \rangle$, and the Fraction of Imaginary Frequencies, F_{imag}, for Xenon Adsorbed in Zeolite-Y[a]

conc.[b] (Xe/s.c.)	T_r[c] (K)	$\langle U \rangle$ (kJ mol^{-1})	D (10^{-8} m^2 s^{-1})	F_{imag}
8	187	−17.8	0.17	0.25
	323	−15.5	0.73	0.40
	398	−14.9	1.04	0.44
	518	−14.0	1.20	0.48
48	120	−16.7	0.03	0.16
	197	−15.2	0.18	0.26
	322	−14.1	0.32	0.32
	411	−13.3	0.43	0.33
	508	−12.8	0.53	0.53

[a] Error bars on $\langle U \rangle$ and F_{imag} are approximately 2%; error bars on D are approximately 10−15%. [b] Concentrations given in terms of Xe atoms per simulation cell. [c] T_r corresponds to the average temperature during a microcanonical MD run.

an increase in temperature for Xe in zeolite-Y (cf. $C_{vv}(t)$ for 8 Xe/s.c. at 187 and 323 K) as well as increase in concentration, the oscillatory character of the autocorrelation function is reduced indicating more rapid decorrelation due to collisions. The short-time dynamics is therefore fairly sensitive to sorbate concentration, temperature, and to a lesser degree to zeolite structure. Table 2 shows the self-diffusion coefficients for Xe in zeolite-Y. Also shown are the F_{imag} values since changes in D and F_{imag} are clearly correlated although no simple proportionality relationship similar to that seen in ionic melts is discernible. Other features of the INM spectra such as the Einstein frequency and the participation ratio appear uncorrelated to D; this is not particularly surprising since the diffusion coefficient is a long-time averaged property of the system. While Table 2 shows only the results for zeolite-Y, results for other zeolites show a similar qualitative correlation between D and F_{imag}.

We first discuss the INM spectra for xenon sorption in different zeolites in the infinite dilution limit. This corresponds to a concentration of one xenon atom per simulation cell. The INM spectrum in this limit represents the curvature distribution of the confining potential. Figure 2 compares the INM spectra in this concentration limit for xenon in different zeolites at 100 K. The double-peaked structure in the real branch for zeolite-A and the shoulder in the case of zeolite-Y can be explained by the peak positions in the underlying QNM spectrum. The qualitative similarity of the four spectra is somewhat deceptive since we show later in this section the sensitivity of various INM features to structural details.

The effect of temperature on the sorbate INM spectrum can be seen for mordenite and zeolite-A in Figure 3, parts a and b, respectively. Also shown in Figure 3 are the quenched normal

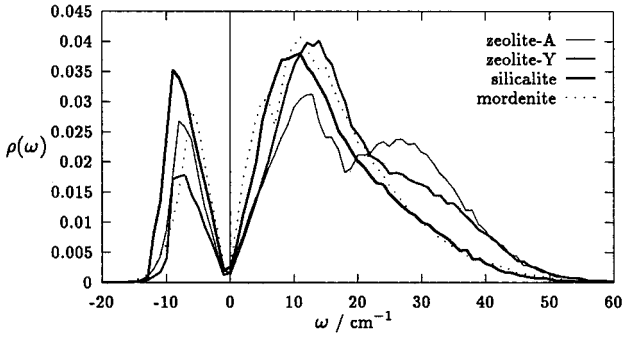

Figure 2. INM spectra of xenon in different zeolites in the infinite dilution limit at 100 K.

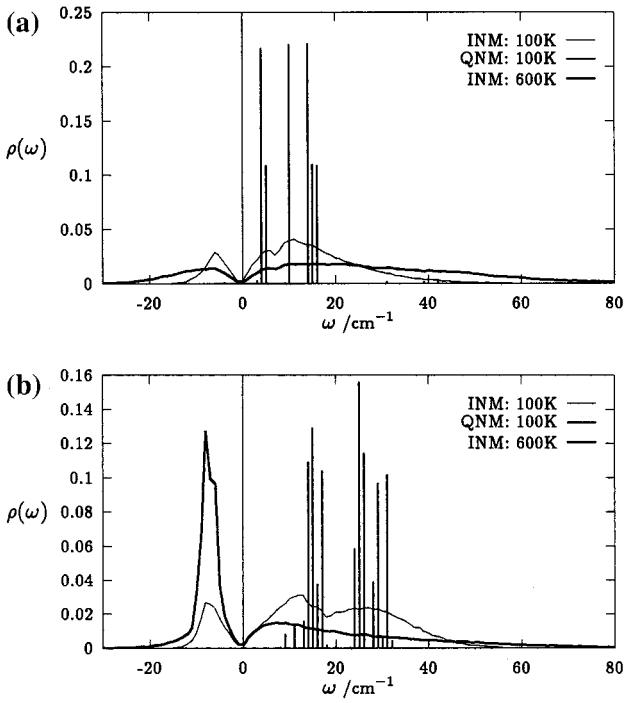

Figure 3. INM and QNM spectra as a function of temperature for xenon adsorbed at infinite dilution in (a) mordenite and (b) zeolite-A.

mode distributions at 100 K. As expected, the INM spectra broaden and lose structure with increase in temperature. Interestingly, the imaginary branch for the two zeolites behaves quite differently. For mordenite it broadens and the peak position shifts appreciably with almost no increase in the F_{imag}, whereas for zeolite-A F_{imag} rises dramatically but the peak position remains virtually unchanged. The QNM distribution for xenon in the different zeolites is almost invariant with temperature and consists of a discrete set of frequencies. This indicates that, in contrast to the situation in clusters and liquids, the system does not possess a set of metastable minima which become accessible with increase in temperature. Clearly the low-temperature adsorption sites remain the only available minima until temperatures of up to 600 K; this is also reflected in the fact that the energies of quenched structure do not change significantly with temperature. As temperature decreases, the INM spectrum develops peaks at frequencies associated with the quenched normal modes.

Behavior of the INM spectra in different zeolite lattices as a function of temperature in the infinite dilution limit is summarized in Figure 4. Figure 4a shows the average guest−host interaction energy, $\langle U_{gh} \rangle$, as a function of temperature for the four zeolites. Since this is a commonly evaluated quantity and is related to the isosteric heat of adsorption, it is a convenient

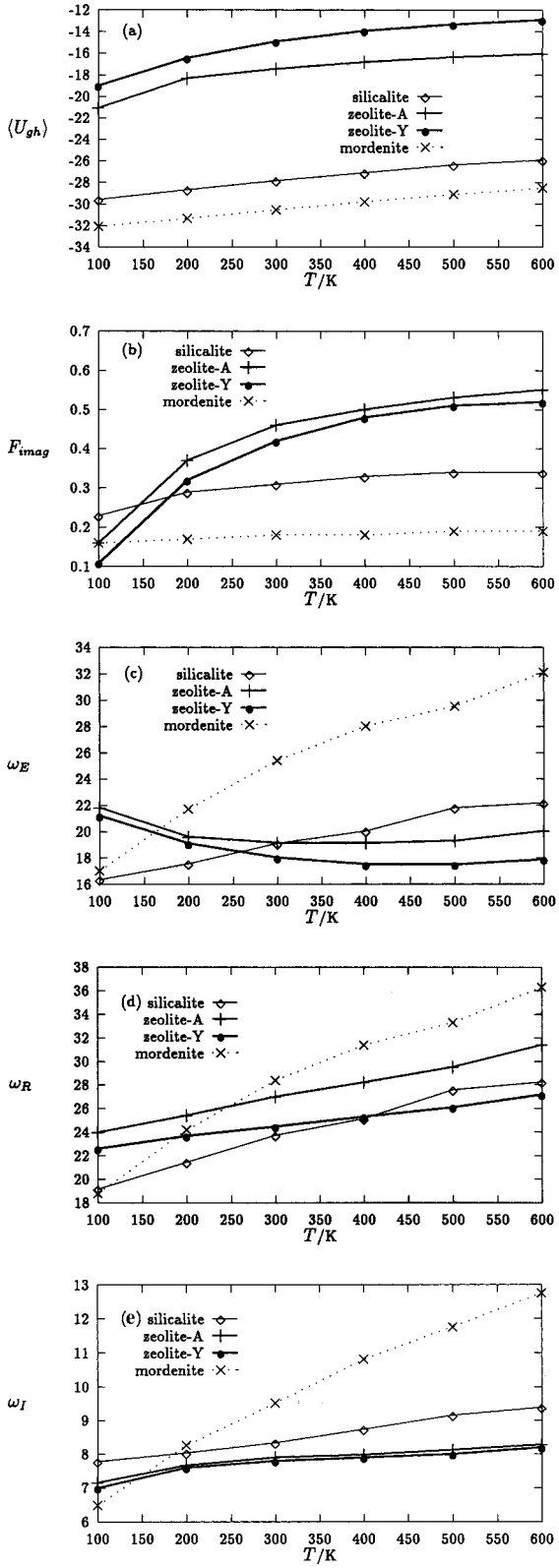

Figure 4. Temperature dependence of various INM-averaged quantities for xenon adsorbed in different zeolites at infinite dilution: (a) average guest−host potential energy, $\langle U_{gh} \rangle$, (b) fraction of imaginary modes in INM spectra, F_{imag}, (c) Einstein frequency, ω_E, (d) average frequency of real branch, ω_R, and (e) average frequency of imaginary branch, ω_I.

check that the PES parameters used here do not introduce any unphysical effects. Note that since we consider the all-silica polymorphs with no framework cations, the relative values of $\langle U_{gh} \rangle$ for the different zeolites at a given temperature correlate with the framework densities given in Table 1. The exception

TABLE 3: INM Features as a Function of Xe Atom Concentration in Zeolite-Y at 300 K[a]

conc[b] (Xe/s.c.)	$\langle U_{gh} \rangle/N$ (kJ mol^{-1})	$\langle U_{gg} \rangle/N$ (kJ mol^{-1})	F_{imag}	ω_E (cm^{-1})	ω_R (cm^{-1})	ω_I (cm^{-1})	$\langle P \rangle$
1	−14.82	0.0	0.42	17.9	24.5	7.8	1.0
8	−15.44	−0.59	0.41	18.7	25.2	7.9	1.2
48	−12.27	−2.07	0.30	40.0	48.2	8.7	2.1
72	−6.53	−2.12	0.23	55.8	63.7	9.3	2.7

[a] Error bars are of the order of 2−4% on the various INM-averaged quantities. [b] Concentrations given in terms of Xe atoms per simulation cell.

is mordenite since the framework densities lead one to expect slightly higher $\langle U_{gh} \rangle$ values in comparison to those for silicalite. This can be explained by the structure of mordenite in which a single xenon atom is preferentially located in the side-pocket sites. Figure 4b shows the fraction of imaginary modes, F_{imag}, as a function of temperature for the different zeolites. Note that at any given temperature above 300 K, F_{imag} decreases with increasing framework density or decreasing the binding energy of the sorbate, with mordenite proving an exception for the structural reason mentioned above. Interestingly, however, for Zeolites-Y, and A, F_{imag} decreases very sharply below 300 K and at 100 K is lower than that for mordenite despite the much greater pore volume in these zeolites. Earlier studies show that at temperatures of 200 K and less, xenon atoms are strongly localized at adsorption sites very close to the walls of the α-cage, whereas above 300 K there is an appreciable probability of finding xenon atoms near the cage center.[40] The qualitative change in the location of xenon atoms in the host is accompanied by this signature in the INM. In contrast, F_{imag} in mordenite is almost constant with temperature since for the temperature range studied the mordenite side pockets are the most favorable sites. Since the mordenite side pockets can contain at most one xenon atom, there is virtually no change in the local environment of a xenon atom with temperature. One would expect that with occupancy of channel sites there would be a significant increase in the fraction of imaginary modes. Figure 4c shows the Einstein frequency, ω_E, as a function of temperature for the four zeolites. The two high-density zeolites show a monotonic increase in the ω_E versus T curve. The two relatively low-density zeolites on the other hand show an increase in ω_E with decrease in temperature below 400 K. Between 400 and 600 K there is a slight increase in the Einstein frequency. The behavior of xenon in zeolites-Y and -A can again be correlated with the change in location of the sorbed atom in the sodalite cages with temperature. Note that ω_E is a measure of the average curvature of the potential rather than the average potential (which is given by $\langle U_{gh} \rangle$). It clearly shows a very different trend with temperature then the simple monotonic behavior of the average guest−host interaction energy. It is also relatively more sensitive to structural differences and does not show a simple correlation with framework density. Figure 4, parts d and e, show the behavior of ω_R and ω_I with temperature and can be seen as an index of the mean positive and negative curvatures, respectively, sampled by the system.

As discussed in the Introduction, we expect that an increase in concentration should decrease the ballistic character of the sorbate dynamics which in turn should be reflected in the INM spectra. Figure 5a shows the INM spectra at concentrations of 8, 48, and 72 Xe atoms in the simulation cell for zeolite-Y at 300 K. Various averaged features of the INM spectrum are given in Table 3. A concentration of 8 Xe/s.c. corresponds to a single Xe atom in each α-cage; Xe−Xe interactions are therefore negligible and the INM spectra are practically undistinguishable

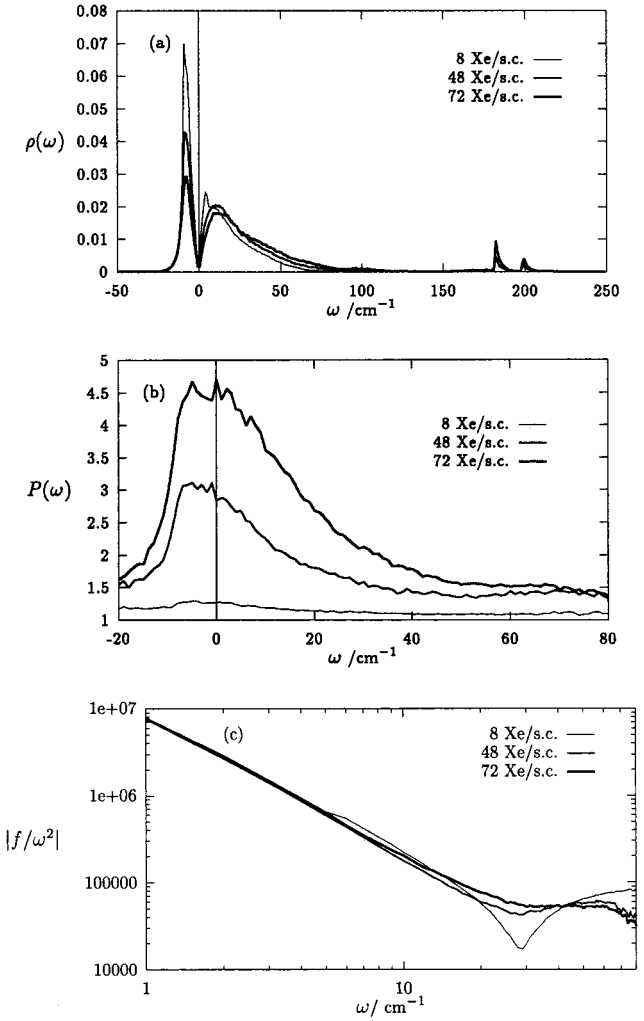

Figure 5. Concentration effects on the INM spectrum of xenon in zeolite-Y: (a) INM spectra, (b) participation ratio distributions, and (c) $|f/\omega^2|$ vs ω on a $\log_{10}/\log_{10}$ scale for the stable INM branch. All simulations are at 300 K. Note that $|f/\omega^2|$ values are given in atomic units.

from the 1 Xe/s.c. results. Increasing the sorbate concentration, however, decreases F_{imag} indicating clustering of Xe atoms in cages. Note that for 72 Xe/s.c., $\langle U_{\mathrm{gh}} \rangle$ is substantially increased because only a few xenon atoms are able to occupy the favorable adsorption sites on the cage periphery. The Einstein frequency increases with concentration partly because of decrease in F_{imag} and partly because of the emergence of two small high-frequency peaks. The most striking effect due to change of concentration is however in the participation ratio distributions which are shown in Figure 5b. In the noninteracting limit (1 Xe/u.c.), $P(\omega)$, is constant at unity. Increasing the concentration to 8 Xe/u.c. lifts the $P(\omega)$ distribution only marginally above unity indicating that the dynamics remains practically unchanged from the infinite dilution limit. Increasing the sorbate concentration to 48 Xe/u.c. (or 6 Xe per α-cage) dramatically lifts $P(\omega)$ for the low-frequency modes. This delocalization of low-frequency modes is further enhanced at a concentration of 72 Xe/u.c. Thus even though rare gas atoms do not form well-defined clusters inside zeolites, the emergence of collective, low-frequency modes is clearly brought out by the participation ratio distributions. While these modes will not display delocalization extending over the entire unit cell, they reflect the fact that increasing concentration within an α-cage promotes slow vibrational motions involving several atoms as opposed to ballistic motion. Figure 5c shows the plot of $|f/\omega^2|$ versus ω on

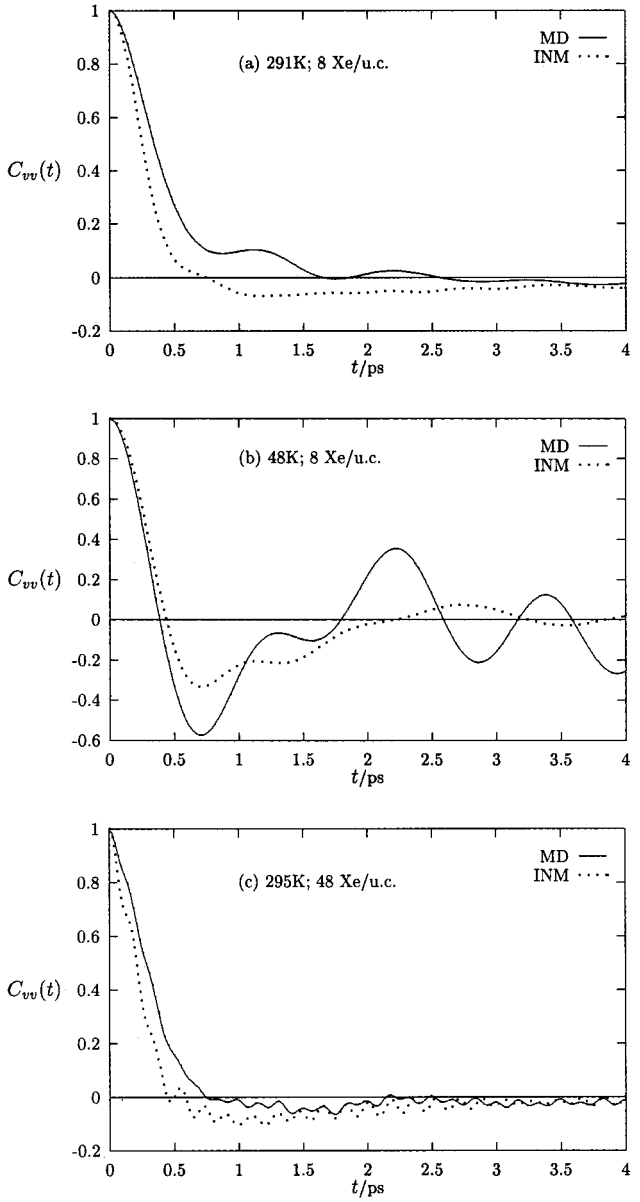

Figure 6. Comparison of the velocity autocorrelation function, $C_{vv}(t)$, from INM and MD data for (a) 8 Xe/u.c. at 291 K, (b) 8 Xe/u.c. at 48 K, and (c) 48 Xe/u.c. at 295 K.

a $\log_{10}/\log_{10}$ scale for the stable INM branch at the three concentrations. This quantity can be thought of as providing a harmonicity test. The anomalous minimum exhibited in the low concentration limit is smoothed away with temperature to give a quasi-linear plot with a slope close to −1.9. However, the INM frequencies for xenon in zeolites stretch over just two decades in frequency rather than three in the case of liquid water. At no concentration studied do we get harmonic behavior with a slope in this plot close to −1. The discrete peaks in the QNM spectra broaden gradually with temperature.

Figure 6 compares the short-time behavior of the velocity autocorrelation function, $C_{vv}(t)$, from the INM expression given in eq 10 as well as directly from the MD simulation. Note that when evaluating the INM expresion, only the stable modes were considered. Figure 6a shows $C_{vv}(t)$ at a concentration of 8 Xe/u.c. and a temperature of 291 K. While for $t < 0.1$ ps, $C_{vv}(t)$ curves obtained by the two methods agree, there is a significant divergence at longer times unlike the situation in simple liquids for which the agreement survives for longer time scales. A possible reason for this could be the high fraction of imaginary

modes (≈40%) under these temperature and concentration conditions. To test this conjecture, Figure 6b shows the two $C_{vv}(t)$ curves for the same concentration but a much lower temperature of 48 K at which the fraction of imaginary modes is practically zero. The agreement between the INM-derived curve and the MD result is now almost exact up to a time of approximately 0.5 ps. Since the fraction of imaginary modes decreases with enhanced concentration as well as decreasing temperature, Figure 6c shows $C_{vv}(t)$ at 295 K for 48 Xe/u.c for which F_{imag} is ≈30%. The agreement between the velocity autocorrelation function derived from MD and INM is now much better than that shown in Figure 6a though not as good as that seen in Figure 6b. The small high-frequency peaks seen in the INM spectrum at approximately 200 cm^{-1} are reflected in the short-time period oscillations seen in the $C_{vv}(t)$ curves obtained from INM as well as from MD data. It should be noted that Figure 1 shows a smoothed version of the $C_{vv}(t)$ curve obtained by sampling at intervals of 0.24 ps rather than 0.024 ps as done in Figure 6.

6. Conclusions

In contrast to the collective diffusional dynamics exhibited by bulk liquids, short-time dynamics in a zeolite, particularly at low sorbate concentrations, is largely ballistic and controlled by the sorbate−wall interactions. A number of interesting features of the INM spectrum emerge in this low concentration regime. There is a high fraction of imaginary frequencies which reflect the curvature distribution of the confining medium and do not necessarily correspond to barrier crossing or diffusional modes. The fraction of imaginary modes increases with temperature and decreases with increase in the strength of sorbate−sorbent binding. A correlation is found between the fraction of imaginary modes and the long-time averaged diffusion coefficient though no simple proportionality relations of the type observed in ionic melts can be deduced. The participation ratios are very close to unity indicating the complete absence of any delocalized or collective modes and reflecting the ballistic character of the short-time dynamics. Qualitative changes in the location of xenon atoms in the α-cages for zeolites-A and -Y with temperature are reflected in the temperature dependence of the fraction of imaginary modes and the Einstein frequency. The average potential energy, however, appears to be insensitive to such changes in the location of xenon atoms. The QNM distribution is almost invariant with temperature and consists of a discrete set of frequencies. This indicates that, in contrast to the situation in clusters and liquids, the system does not possess a set of metastable minima which become accessible with increase in temperature. The two INM features which behave differently for xenon in zeolite, particularly at low concentrations, when compared with liquids, are the harmonicity ratio and the short-time velocity autocorrelation function computed from the INM spectrum. While $C_{vv}(t)$ obtained from INM and MD must agree as $t \rightarrow 0$, the time period for which the agreement survives was found to be strongly dependent on concentration and temperature. In general, the agreement improves if simulation conditions are chosen so as to reduce the fraction of imaginary modes. The plot of $|f_i/\omega_i^2|$ versus ω_i on a $\log_{10}/\log_{10}$ scale for the stable INM branch does not show the expected slope of −1 for a perfectly harmonic system but an approximate slope of −1.9.

With increasing concentration, we expect the onset of liquidlike behavior even though the strong guest−host interaction in a zeolite cavity will tend to prevent formation of well-defined clusters.[39] However, the emergence of delocalized, collective motions in the short-time dynamics is clearly shown by the rise in the participation ratio of the low-frequency modes. These relatively delocalized vibrations can arise only when there are an appreciable number of atoms in a given zeolite cage. At any given temperature, the fraction of imaginary modes decreases with increasing concentration and is accompanied by a decrease in the diffusion coefficients calculated from MD simulations. The deviations from linearity in the log−log plot of $|f/\omega^2|$ versus ω are smoothed away with increasing concentration. The Einstein frequency shows a different trend from the average potential energy; for example, it increases with concentration though the overall average binding energy per atom actually decreases above a certain concentration. The increased complexity of the underlying PES with concentration is reflected in the quenched energies and QNM spectra which lose their discrete character.

From the INM analysis of sorbate dynamics in zeolites presented in this paper, we conclude that certain features of the INM spectrum should be interesting indicators of the effect of confinement on the short-time dynamics of a fluid. In particular, the participation ratio distribution is a good indicator both of the emergence of collective vibrational modes and the degree of ballistic character of the short-time dynamics. Another INM property which seems specially sensitive to concentration and strength of confinement is the harmonicity ratio. A comparison of the INM spectra of the adsorbed fluid at infinite dilution with that for the pure liquid as well as that for the confined fluid can reveal qualitative differences in the dynamics. We therefore expect that instantaneous normal mode analysis will provide a useful diagnostic for simulation studies of adsorption in random and ordered porous media.

Acknowledgment. This work was supported by the Department of Science and Technology, New Delhi (Grant No. SP/S1/H-36/94) and the Indian National Science Academy.

References and Notes

(1) Barrer, R. M. *Zeolites and Clay Minerals as Sorbents and Molecular Sieves*; Academic Press: New York, 1978.
(2) Breck, D. W. *Zeolite Molecular Sieves*; Wiley-Interscience: New York, 1974.
(3) Demontis, P.; Suffriti, G. B. *Chem. Rev.* **1997**, *97*, 2845.
(4) Nicholson, D. *Faraday Trans. Chem. Soc.* **1996**, *92*, 1.
(5) Cracknell, R. F.; Gubbins, K. E.; Maddox, M.; Nicholson, D. *Acc. Chem. Res.* **1995**, *28*, 281.
(6) Gubbins, K. E.; Sliwinskabartkowiak, M.; Suh, S. H. *Mol. Simul.* **1996**, *17*, 333.
(7) Kärger, J.; Ruthven, D. M. *Diffusion in Zeolites and Other Microporous Solids*; Wiley: New York, 1992.
(8) Boddenberg, B.; Beerwerth, B. *J. Chem. Phys.* **1989**, *93*, 1440.
(9) Bull, L. M.; Henson, N. J.; Cheetham, A. K.; Newsam, J. M.; Heyes, S. J. *J. Phys. Chem.* **1993**, *97*, 11776.
(10) Dybowski, C.; Bansal, N.; Duncan, T. M. *Annu. Rev. Phys. Chem.* **1991**, *42*, 433.
(11) Barrie, P. J.; Klinowski, J. *Prog. NMR Spectrosc.* **1992**, *24*, 91.
(12) Stratt, R. M.; Marconelli, M. *J. Phys. Chem.* **1996**, *100*, 12981.
(13) Stratt, R. M. *Acc. Chem. Res.* **1995**, *28*, 201.
(14) Buchner, M.; Ladanyi, B. M.; Stratt, R. M. *J. Chem. Phys.* **1992**, *97*, 8522.
(15) Bembenek, S. D.; Laird, B. B. *Phys. Rev. Lett.* **1995**, *74*, 936.
(16) Zwanzig, R. *J. Chem. Phys.* **1983**, *79*, 4507.
(17) Seeley, G.; Keyes, T. *J. Phys. Chem.* **1989**, *91*, 5581.
(18) Keyes, T. *J. Chem. Phys.* **1997**, *106*, 46.
(19) Vijayadamodar, G. V.; Nitzan, A. *J. Chem. Phys.* **1995**, *103*, 2169.
(20) Sastry, S. *Phys. Rev. Lett.* **1996**, *76*, 3738.
(21) Gezelter, J. D.; Rabani, E.; Berne, B. J. *J. Chem. Phys.* **1997**, *107*, 4618.
(22) Cho, M.; Fleming, G. R.; Saito, S.; Ohmine, I.; Stratt, R. M. *J. Chem. Phys.* **1994**, *100*, 6672.
(23) Adams, J. E.; Stratt, R. M. *J. Chem. Phys.* **1990**, *93*, 1358; Adams, J. E.; Stratt, R. M. *J. Chem. Phys.* **1990**, *93*, 1632.
(24) Vallauri, R.; Bermejo, F. J. *Phys. Rev. E.* **1995**, *51*, 2654.

(25) Wu, T.-M.; Tsay, S.-F. *J. Chem. Phys.* **1996**, *105*, 9281.
(26) Ribeiro, M. C. C.; Madden, P. A. *J. Chem. Phys.* **1997**, *106*, 8616.
(27) Buch, V. *J. Phys. Chem.* **1990**, *93*, 2631.
(28) Chakravarty, C.; Ramaswamy, R. *J. Chem. Phys.* **1997**, *106*, 5564.
(29) Cao, J.; Voth, G. A. *J. Chem. Phys.* **1994**, *101*, 6184.
(30) Allen, M. P.; Tildesley, D. J. *Computer Simulation of Liquids*; Clarendon Press: Oxford, 1987.
(31) Frenkel, D.; Smit, B. *Understanding Molecular Simulation: From Algorithms to Applications*; Academic Press: London, 1996.
(32) Stillinger, F. H.; Weber, T. A. *Science* **1984**, *225*, 983.
(33) Chakravarty, C.; Thiruvengadaravi, K. V. *Proceedings of the conference on "Frontiers in Materials Modelling and Design"*; 20−23 August 1996, Kalpakkam; Springer-Verlag: Berlin, 1997.
(34) Chakravarty, C. *J. Phys. Chem.* **1997**, *100*, 1878.
(35) Chitra, R.; Yashonath, S. *Proc. Ind. Acad. Sci. Chem. Sci.* **1997**, *109*, 189.
(36) Bezus, A. G.; Kiselev, A. V.; Lopatkin, A. A.; Du, P. Q. *J. Chem. Soc., Faraday Trans. 2* **1978**, *74*, 367.
(37) Kiselev, A. V.; Du, P. Q. *J. Chem. Soc., Faraday Trans. 2* **1981**, *77*, 1.
(38) Kiselev, A. V.; Lopatkin, A. A.; Shulga, A. A. *Zeolites* **1985**, *5*, 261.
(39) Chitra, R.; Yashonath, S. *J. Phys. Chem. B* **1997**, *101*, 5437.
(40) Yashonath, S.; Santikary, P. *Phys. Rev. B* **1992**, *45*, 10095; Yashonath, S.; Santikary, P. *Phys. Rev. B* **1994**, *98*, 6368.
(41) Amrani, S. E.; Vigne-Maeder, F.; Bigot, B. *J. Phys. Chem.* **1992**, *96*, 9417.
(42) Demontis, P.; Suffriti, G. B.; Tilocca, A. *J. Chem. Phys.* **1986**, *105*, 5586.
(43) Lermer, H.; Draeger, M.; Steffen, J.; Unger, K. K. *Zeolites* **1985**, *5*, 131.
(44) Meier, W. M.; Olson, D. H. *Atlas of Zeolite Structure Types*; Butterworth: Boston, 1988.
(45) Bibby, D. M.; Dale, M. P. *Nature* **1985**, *317*, 15.
(46) Vigne-Maeder, F. *J. Phys. Chem.* **1994**, *98*, 4666.
(47) Fitch, A. N.; Jobic, H.; Renouprez, A. J. *J. Phys. Chem.* **1986**, *90*, 1311.
(48) Pluth, J. J.; Smith, J. V. *J. Am. Chem. Soc.* **1980**, *102*, 4704.
(49) Treacy, M. M. J.; Higgins, J. B.; von Ballmoos, R. *Zeolites* **1996**, *16*, 751.
(50) Hirschfelder, O. J.; Curtiss, F. C.; Bird, B. R. *Molecular Theory of Gases and Liquids*; John Wiley: Chichester, 1954.
(51) Bell, R. J.; Dean, P. *Faraday Trans. Chem. Soc.* **1970**, *50*, 55.
(52) Press, W. H.; Flannery, B. P.; Teukolsky, S. A.; Vetterling, W. T. *Numerical Recipes: The Art of Scientific Computing*; Cambridge University Press: New York, 1989.